Supporting Information

Exploring the effects of different crosslinkers on lignin-based thermoset properties and morphologies

Iuliana Ribca[1,2], Marcus E. Jawerth[1,2], Calvin J. Brett[1,2,3,4], Martin Lawoko[1], Matthias Schwartzkopf[4], Andrei Chumakov[4], Stephan V. Roth[2,4], and Mats Johansson[1,2,*]

[1] KTH Royal Institute of Technology, Department of Fiber and Polymer Technology, Wallenberg Wood Science Center (WWSC), Teknikringen 56-58, SE-10044 Stockholm, Sweden

[2] KTH Royal Institute of Technology, Department of Fiber and Polymer Technology, Division of Coating Technology, Teknikringen 56-58, SE-10044 Stockholm, Sweden

[3] KTH Royal Institute of Technology, Department of Engineering Mechanics, Teknikringen 8, 10044 Stockholm, Sweden

[4] Deutsches Elektronen-Synchrotron (DESY), Notkestrasse 85, 22607 Hamburg, Germany

*Corresponding Author, e-mail: matskg@kth.se

- Number of pages: 15
- Number of figures: 21
- Number of schemes: 1
- Number of tables: 3

Table of Contents

Fractionation and Characterization of Raw Material

Table S1. ICP-OES Analysis of LignoBoost Kraft Lignin Before and After Washing Process.

Inorganics (ppm)	KL	KL_Washed
S	30460 ± 390	16560 ± 145
Na	1137 ± 132	79 ± 6
Mg	132 ± 23	109 ± 2
K	115 ± 6	31 ± 3
Ca	83 ± 0.5	51 ± 0.5
Mn	76 ± 2	66 ± 1
Al	67 ± 1	57 ± 0.5
Fe	51± 1	37 ± 1
Zn	40 ± 3	31 ± 3
P	20 ± 1	16 ± 1
Cu	9 ± 1	3 ± 0.5
Cr	4 ± 0.1	4 ± 0.01

Scheme S1. Schematic Representation of the Sequential Solvent Fractionation.

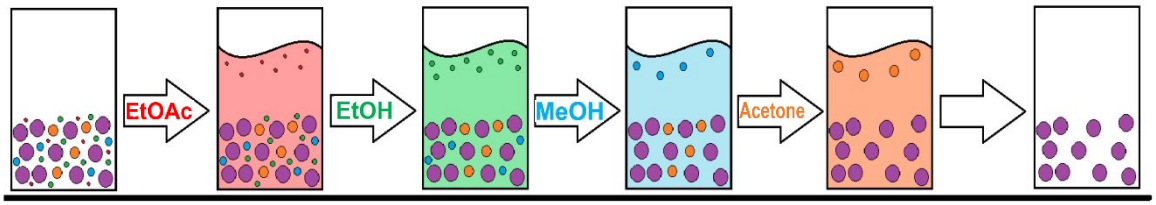

Table S2. Yield of Different Lignin Fractions. Number/Weight Average Molar Mass and Polydispersity of Different Lignin Fractions Determined by SEC.

	Yield %	M_n g/mol	M_w g/mol	$Đ$
KL_Initial	-	650	5750	8.8
KL_EtOAc	20	250	750	3.1
KL_EtOH	24	650	1900	2.9
KL_MeOH	9	1300	2750	2.1
KL_Acetone	10	2250	4000	1.8
KL_Insoluble	34	7400	22400	3.0

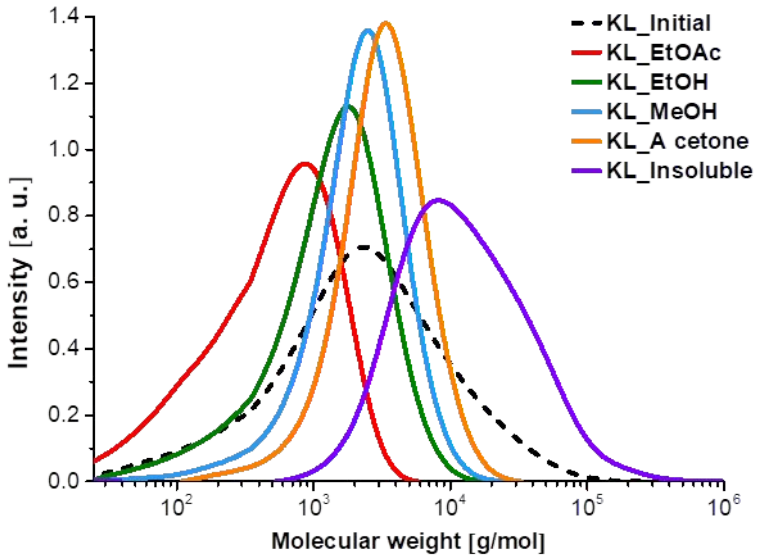

Figure S1. Molar mass distribution of fractionated lignin. The dotted line represents the LignoBoost Kraft lignin before washing.

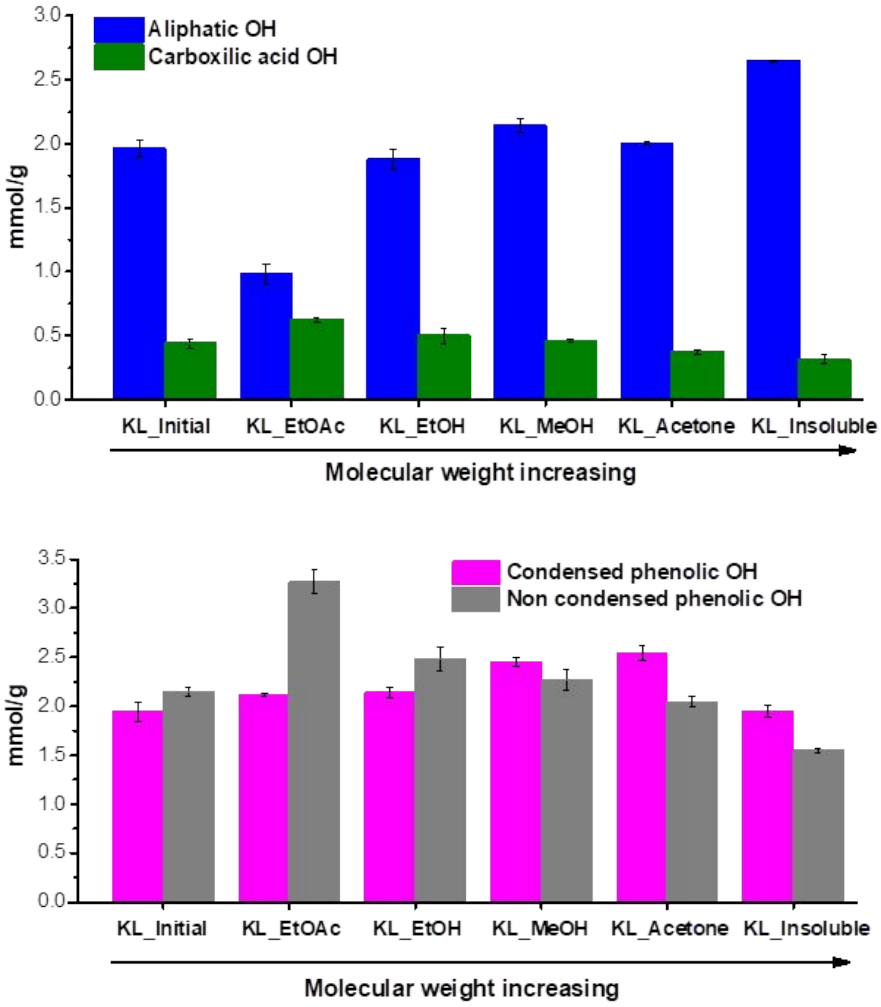

Figure S2. The amounts of different OH functionalities determined by ^{31}P NMR.

Table S3. Integration Region for OH Functional Groups in ^{31}P NMR Spectrum.[1-3]

Functional group	Chemical shift (ppm)
Aliphatic OH	149.5 – 145.5
Phenolic OH	144.7 – 137.0
Condensed phenolic OH	144.7 – 140.1
Non-condensed phenolic OH	140.1 – 138.8
Catechol	138.8 – 138.2
p-hydroxyphenyl	138.2 – 137.0
Carboxylic acid OH	136.0 – 133.6

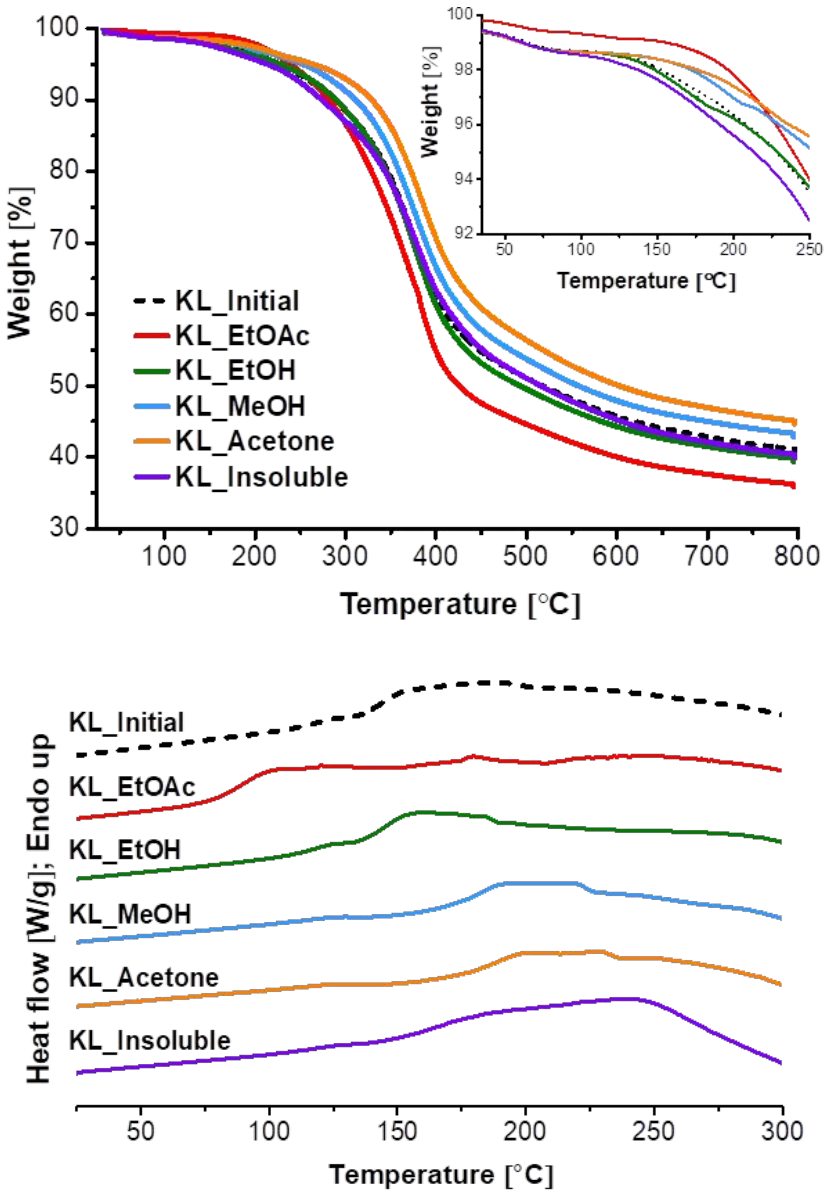

Figure S3. TGA (top) and DSC (bottom) thermograms of the initial and fractionated lignin.

Selective Allylation of Ethanol Soluble Fraction

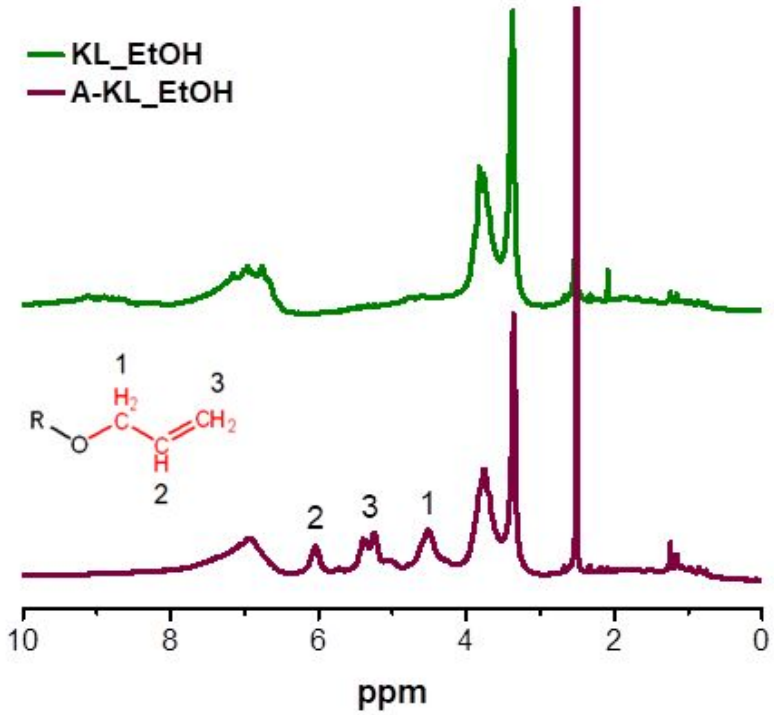

Figure S4. ^{1}H NMR spectra of KL_EtOH (top) and A-KL_EtOH (bottom). The signals at 3.37 ppm and 2.50 ppm are attributed to H_2O and deuterated solvent.

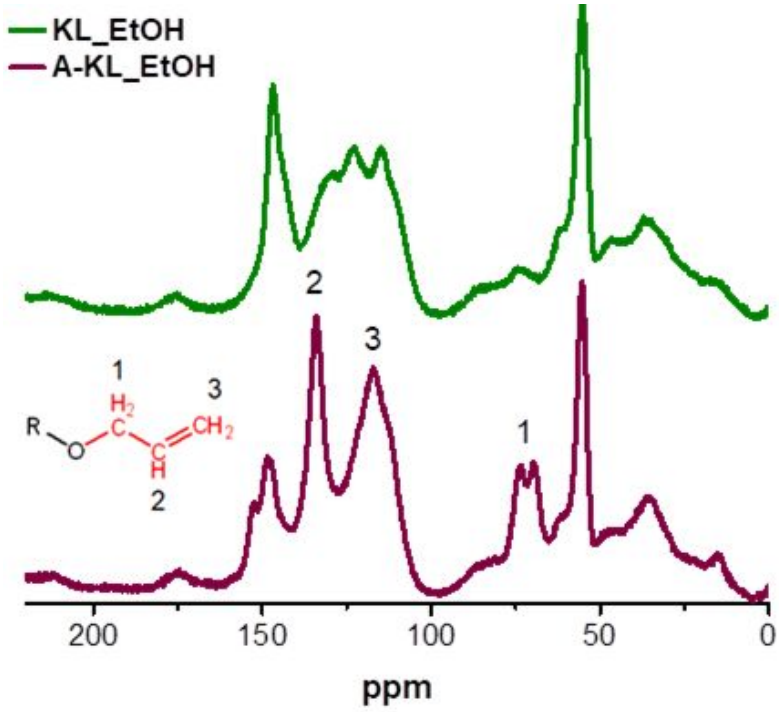

Figure S5. Solid-state CP/MAS ^{13}C NMR spectra of ethanol soluble fraction (green line) and allylated lignin (red line).

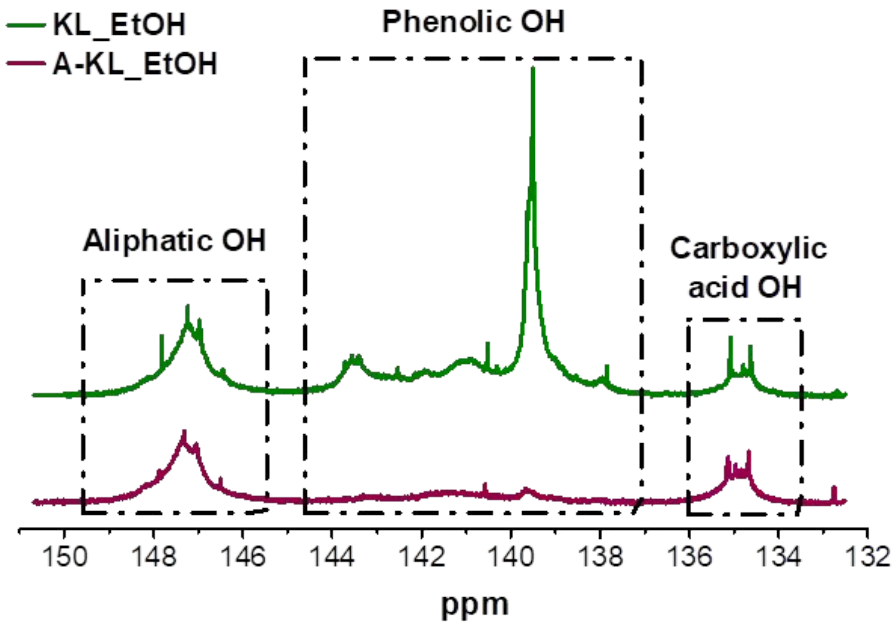

Figure S6. Quantitative ^{31}P NMR spectra of KL_EtOH (top) and allylated KL_EtOH (bottom).

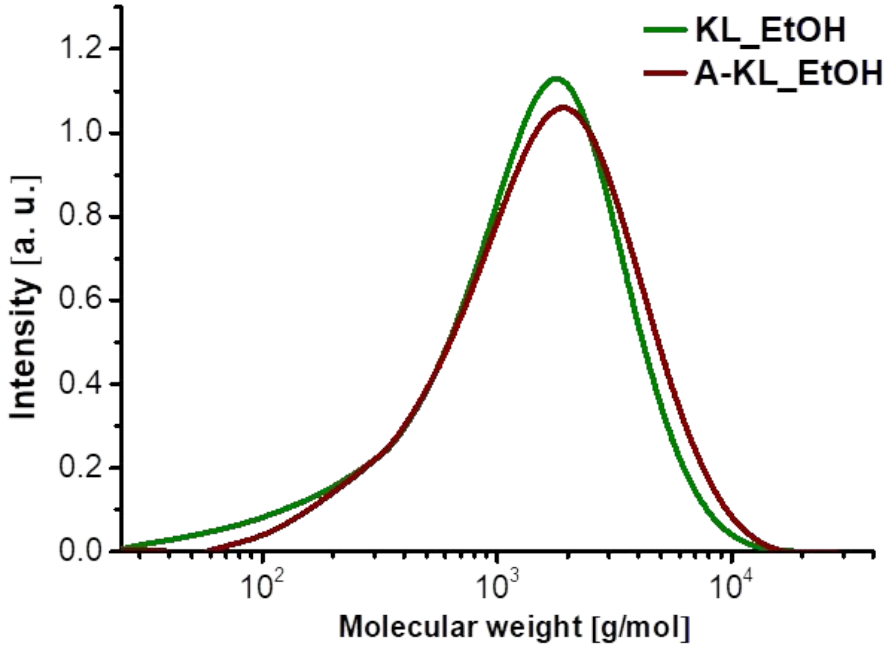

Figure S7. Molar mass distribution of ethanol soluble fraction and allylated lignin.

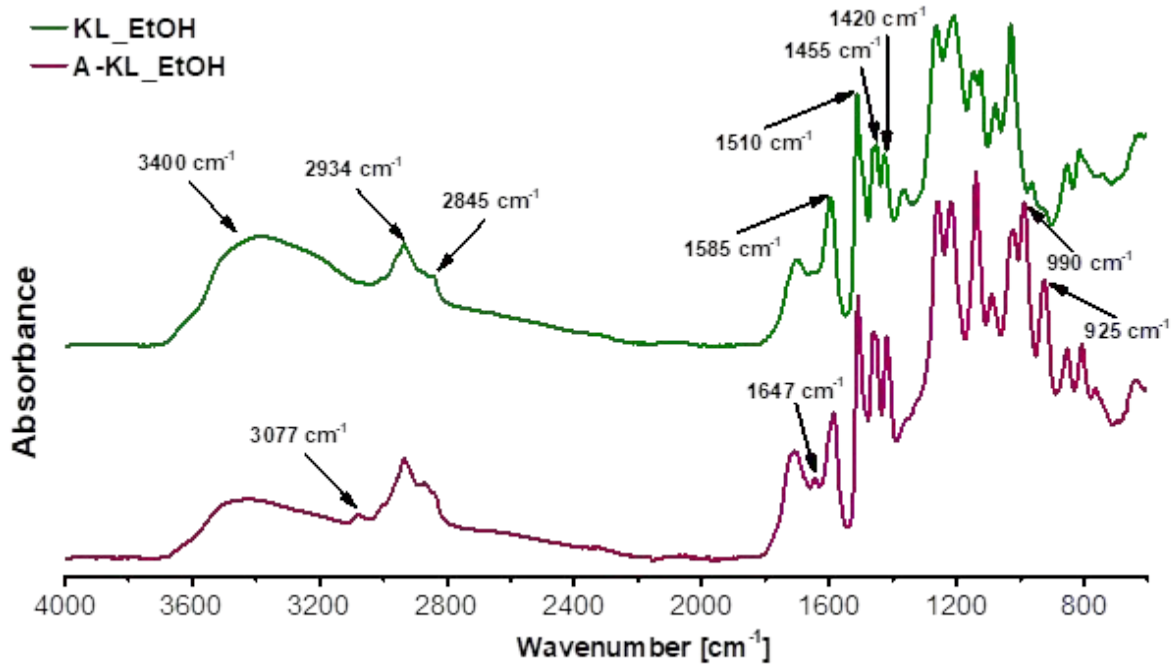

Figure S8. FT-IR (ATR) spectra of unmodified ethanol soluble fraction (top) and allylated lignin (bottom). The spectra were shifted for better visualization.

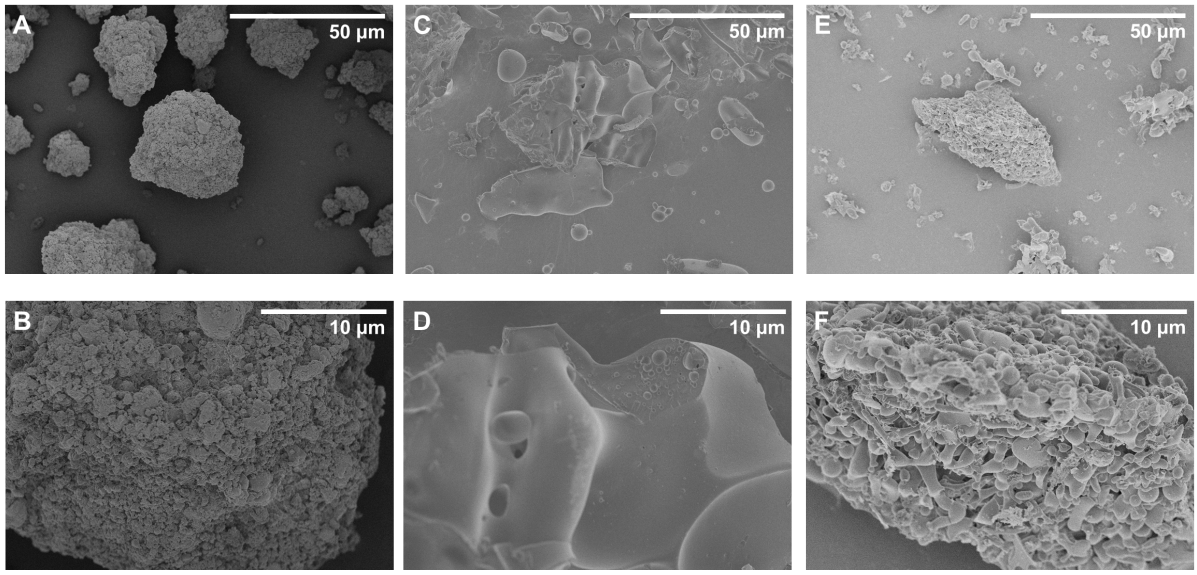

Figure S9. Representative SEM images of the initial lignin (KL_Initial: A,B), the ethanol soluble fraction (KL_EtOH: C, D), and the allylated lignin (A-KL_EtOH: E, F) at lower magnification (top row) and at higher magnification (bottom row).

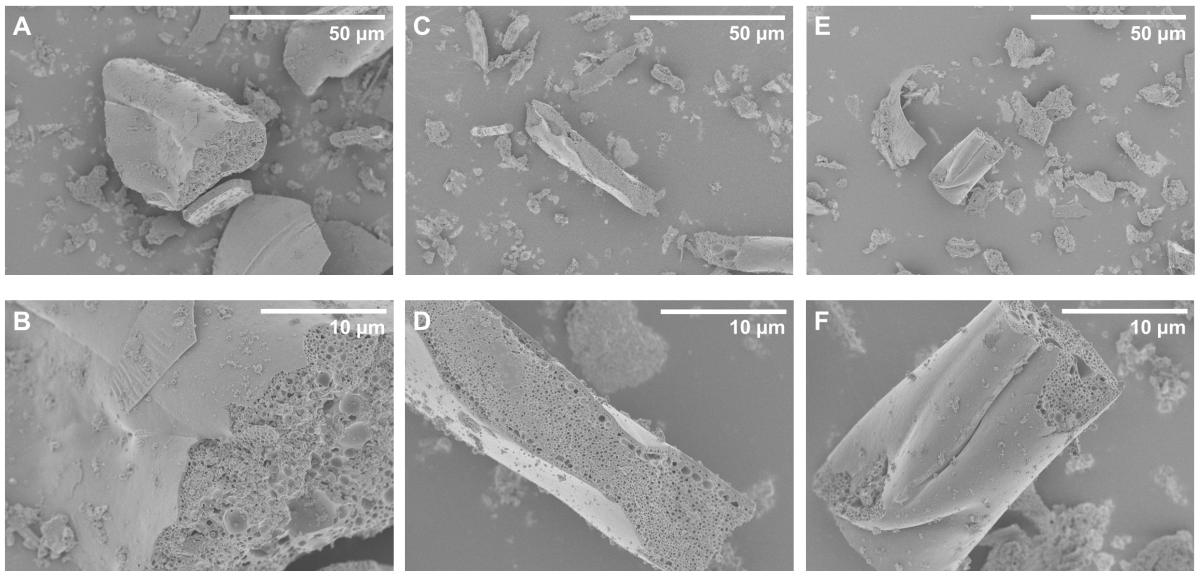

Figure S10. Representative SEM images of freeze-dried KL_EtOH at lignin concentration ≈7 mg/mL at higer magnification (A, C, E) and at lower magnification (B, D, F).

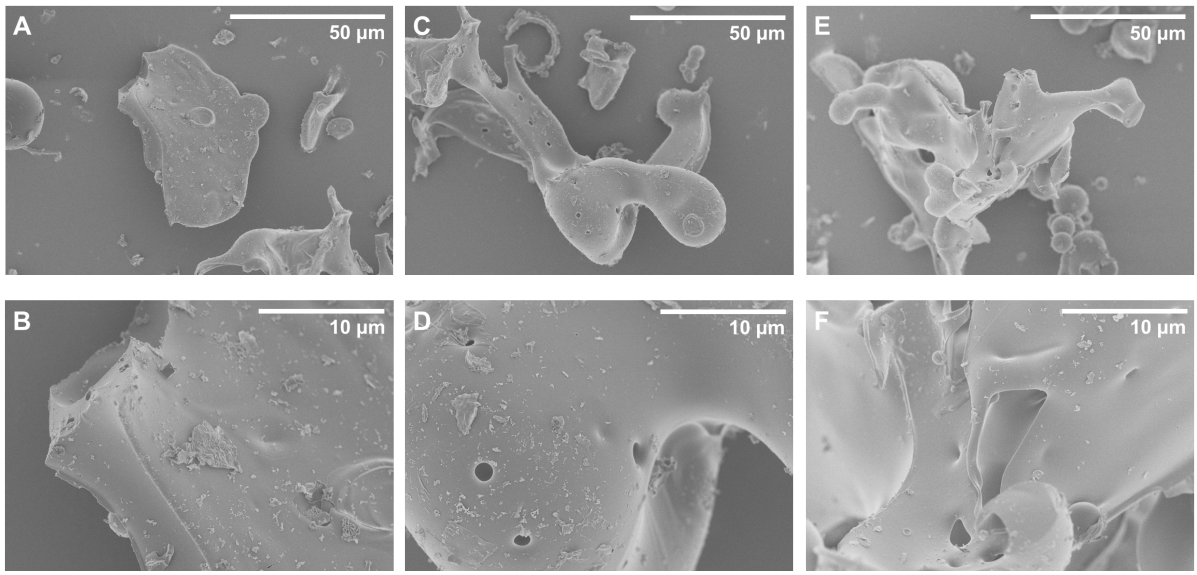

Figure S11. Representative SEM images of freeze-dried KL_EtOH at lignin concentration ≈40 mg/mL at higer magnification (A, C, E) and at lower magnification (B, D, F).

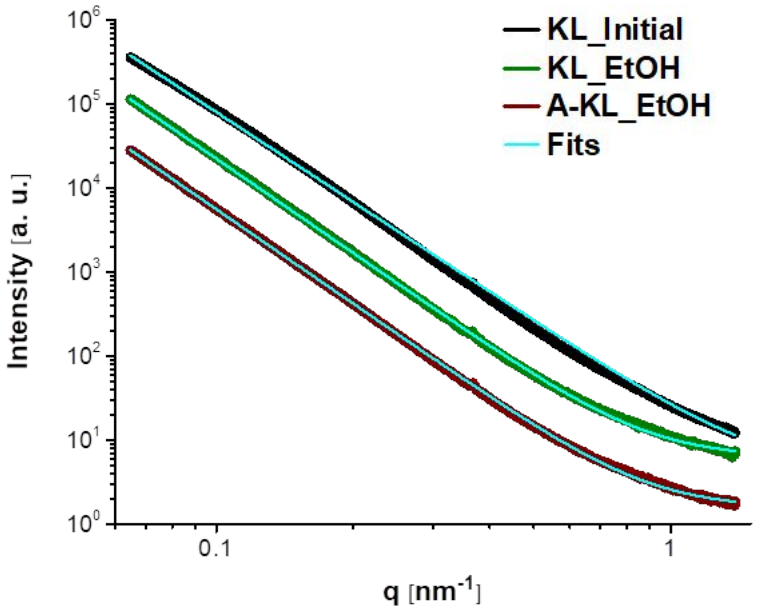

Figure S12. The 1D scattering intensities *I(q)* and corresponding fits of KL_Initial, KL_EtOH, and A-KL_EtOH. For better visualization the A-KL_EtOH curve was slightly shifted with respect to KL_EtOH.

Curing Performance of Allylated Lignin Resins Using Different Thiol Crosslinkers

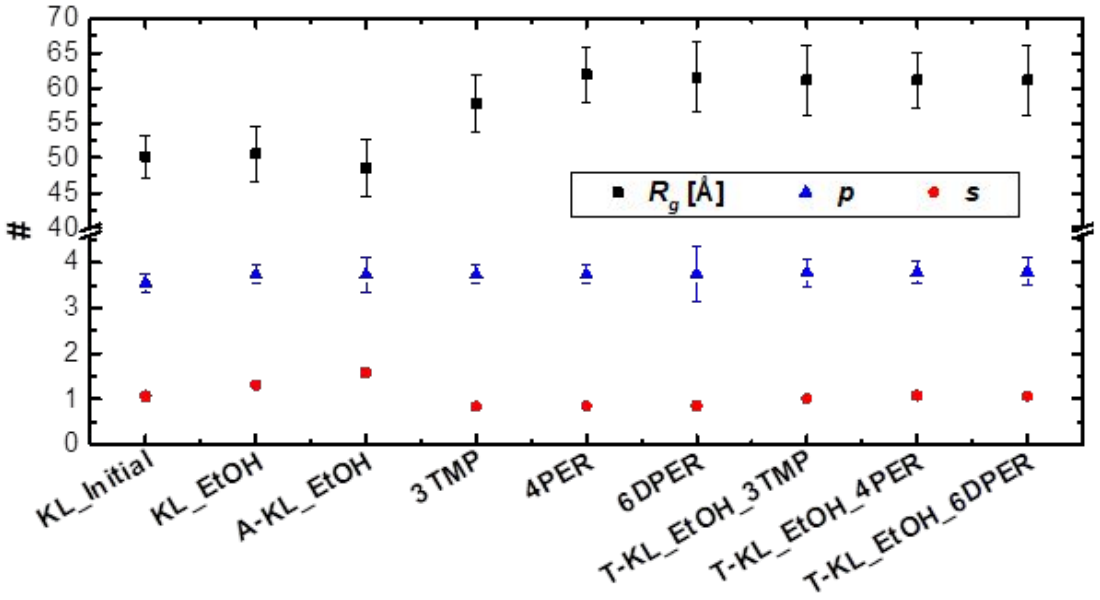

Figure S13. SAXS fitting results from the Guinier-Porod model assumption for powdery lignin, crosslinkers and thermosets. The Guinier radius R_g shows the sizes of the observed structures. The dimensionality parameter s gives information regarding the structure and the Porod exponent p about the surface character if it is a rather smooth or rough surface.[3]

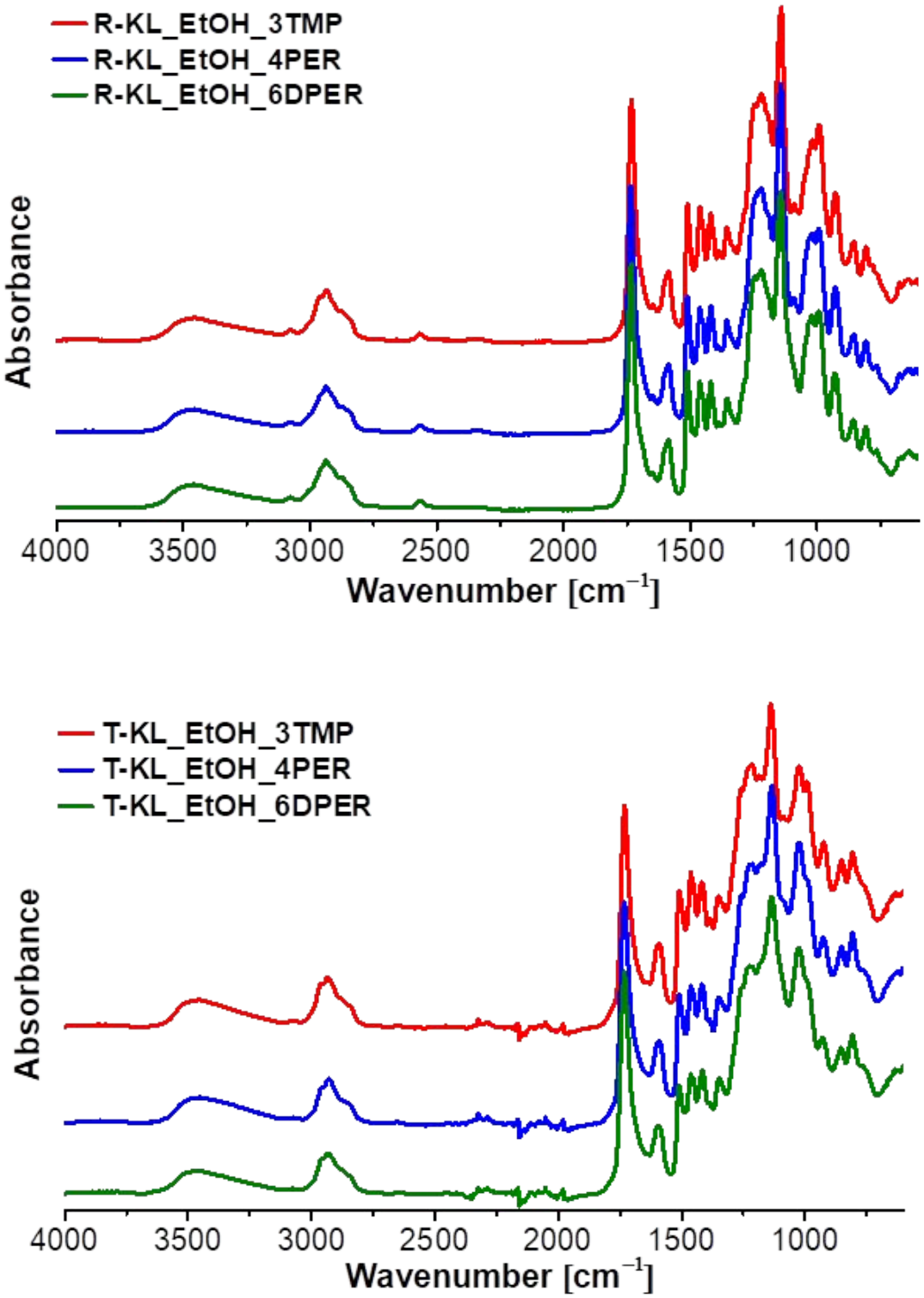

Figure S14. FT-IR spectra of resins mixed with the three specific crosslinkers before (top) and after (bottom) curing process. The spectra were shifted for better visualization.

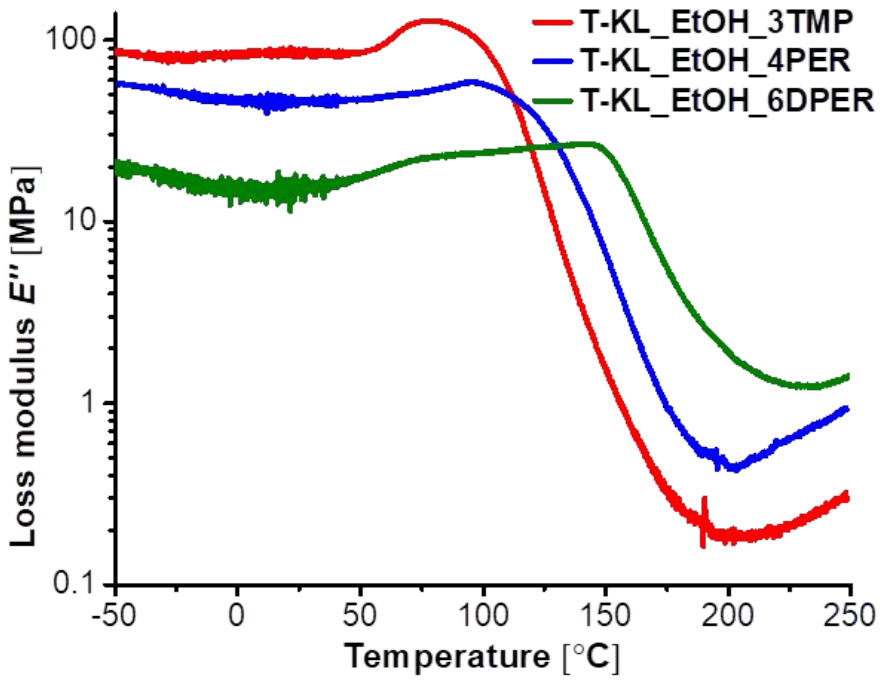

Figure S15. Loss modulus for the cured resins obtained by DMA analysis.

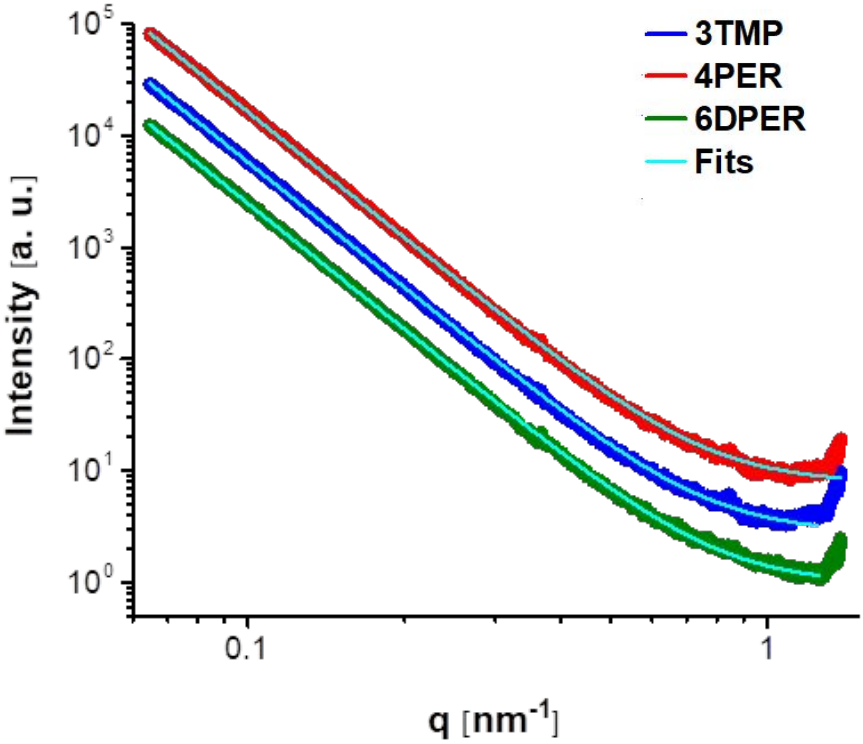

Figure S16. The 1D scattering intensities *I(q)* and corresponding fits of 3TMP, 4PER, and 6DPER. For better visualization the 3TMP and 4PER curves were slightly shifted with respect to 6DPER.

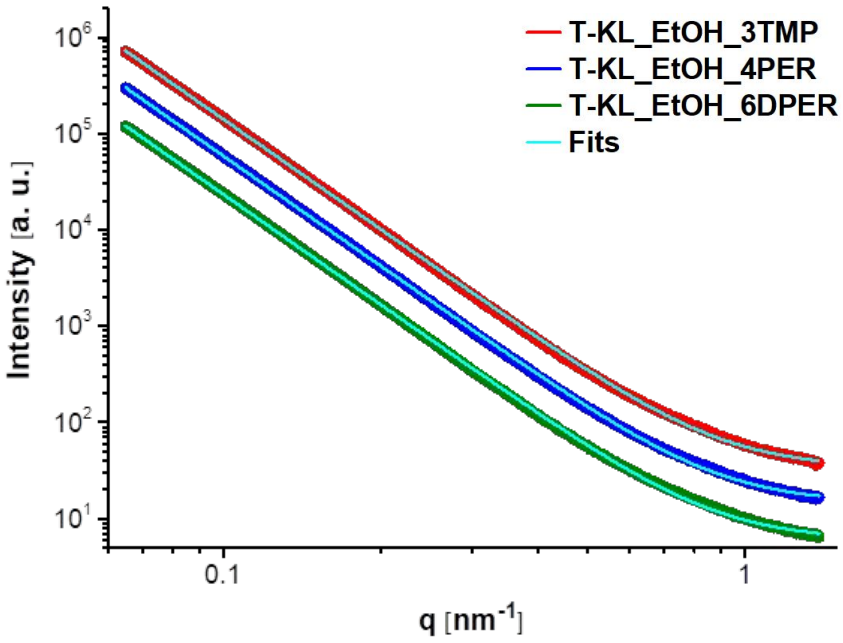

Figure S17. The 1D scattering intensities *I(q)* and corresponding fits of three different thermosets. For better visualization the T-KL_EtOH_3TMP and T-KL_EtOH_4PER curves were slightly shifted with respect to T-KL_EtOH_6DPER.

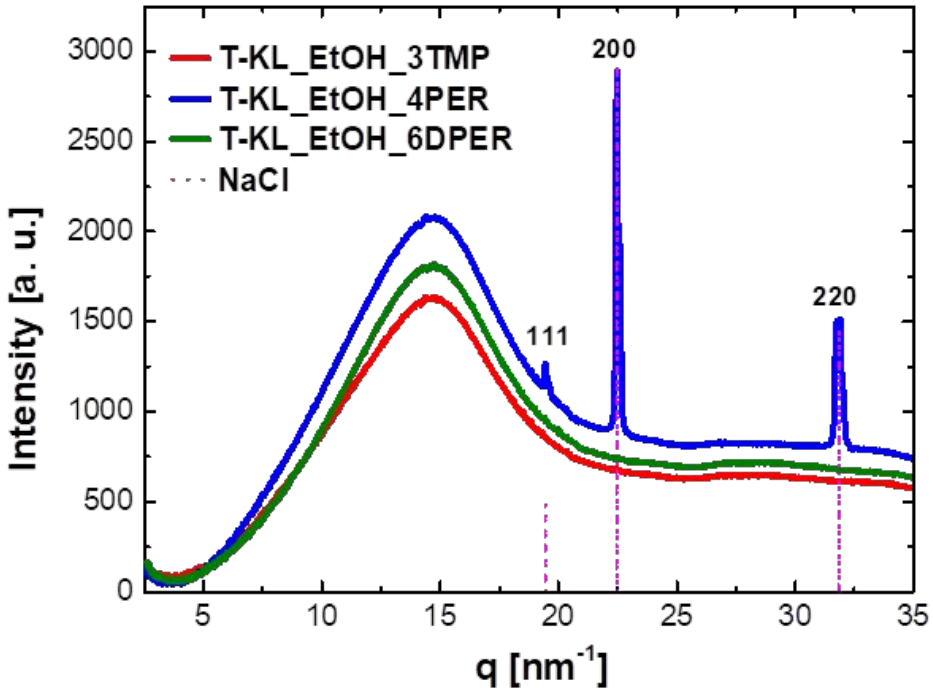

Figure S18. WAXS scattering intensity for thermosets extracted from the two-dimensional scattering patterns. On the T-KL_EtOH_4PER sample (blue) three peaks can be observed in the range of 5 nm^{-1} to 35 nm^{-1}. The assigned sharp peaks originate from NaCl from the washing step during the allylation procedure.

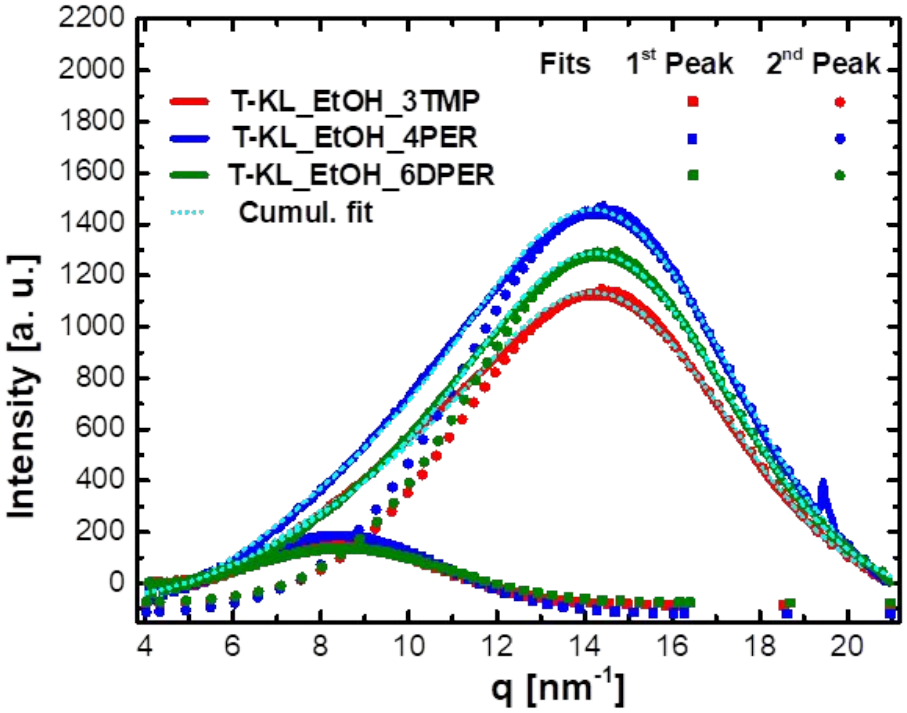

Figure S19. The amorphous peak presented in Figure S14 was fitted with Gaussian functions to yield the peak position as well as the content of the different representations of π- π-stacking in the sample.

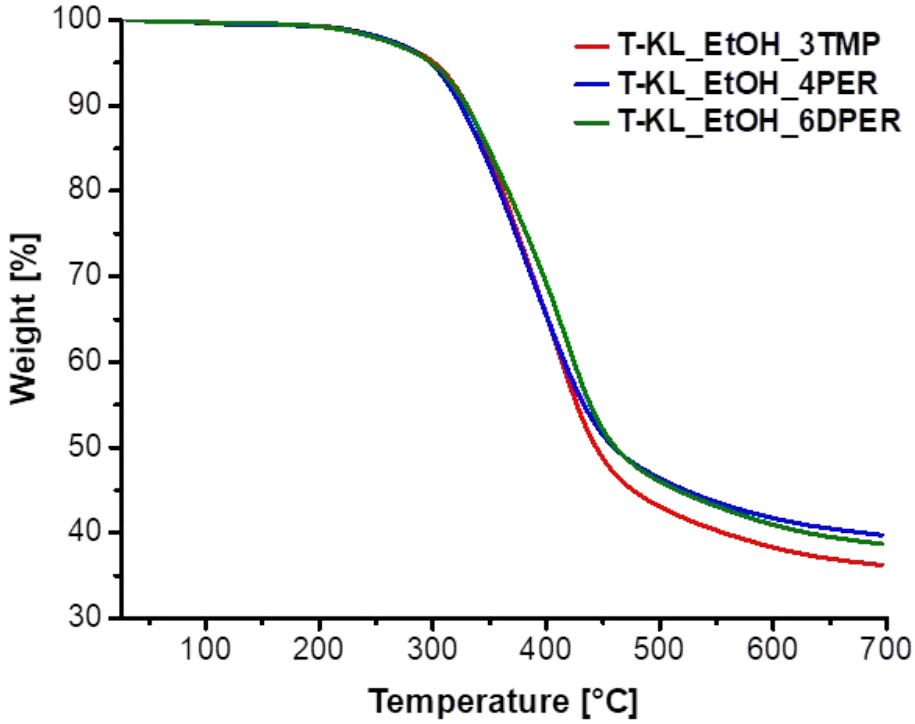

Figure S20. TGA curves of lignin-based thermosets.

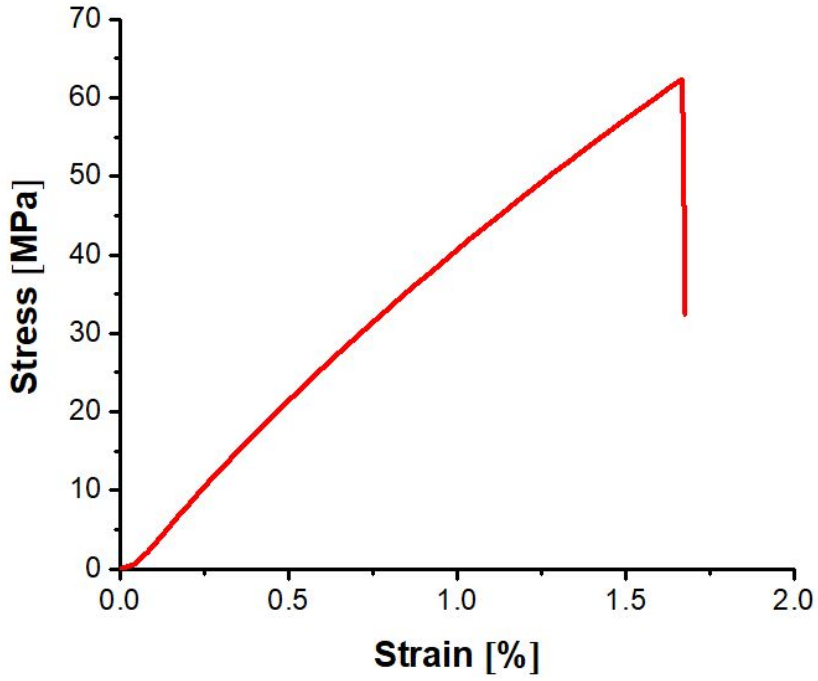

Figure S21. Representative stress-strain curve for the T-KL_EtOH_3TMP sample.

References

1. Meng, X.; Crestini, C.; Ben, H.; Hao, N.; Pu, Y.; Ragauskas, A. J.; Argyropoulos, D. S., Determination of hydroxyl groups in biorefinery resources via quantitative 31P NMR spectroscopy. *Nat. Protoc.* **2019,** *14* (9), 2627-2647 DOI: https://doi.org/10.1038/s41596-019-0191-1

2. Granata, A.; Argyropoulos, D. S., 2-Chloro-4,4,5,5-tetramethyl-1,32-dioxaphospholane, a Reagent for the Accurate Determination of the Uncondensed and Condensed Phenolic Moieties in Lignins. *J. Agric. Food. Chem.* **1995,** *43* (6), 1538-1544 DOI: https://doi.org/10.1021/jf00054a023

3. Argyropoulos, D., Quantitative Phosphorus-31 NMR Analysis of Six Soluble Lignins. *J. Wood Chem. Technol.* **1994,** *14* (1), 65-82 DOI: http://dx.doi.org/10.1080/02773819408003086